

Article

Nitrogen-Doped Ordered Mesoporous Carbons Supported Co_3O_4 Composite as a Bifunctional Oxygen Electrode Catalyst

Jing Wang ¹, Shuwei Zhang ¹, Haihong Zhong ^{1,2}, Nicolas Alonso-Vante ² , Dianqing Li ¹, Pinggui Tang ¹ and Yongjun Feng ^{1,*} 

¹ State Key Laboratory of Chemical Resource Engineering, Beijing Engineering Center for Hierarchical Catalysts, Beijing University of Chemical Technology, No. 15 Beisanhuan East Road, Beijing 100029, China; 2017200993@buct.edu.cn (J.W.); 2016201069@buct.edu.cn (S.Z.); 2014200922@grad.buct.edu.cn (H.Z.); lidq@mail.buct.edu.cn (D.L.); tangpg@mail.buct.edu.cn (P.T.)

² IC2MP, UMR-CNRS 7285, University of Poitiers, F-86022 Poitiers CEDEX, France; nicolas.alonso.vante@univ-poitiers.fr

* Correspondence: yjfeng@mail.buct.edu.cn; Tel.: +86-10-6442-5385

Received: 20 February 2019; Accepted: 26 March 2019; Published: 29 March 2019



Abstract: It is increasingly useful to develop bifunctional catalysts for oxygen reduction and oxygen evolution reaction (ORR and OER) for fuel cells, metal-air rechargeable batteries, and unitized regenerative cells. Here, based on the excellent conductivity and stability of ordered mesoporous carbons, and the best ORR and OER activity of Co_3O_4 , the composite $\text{Co}_3\text{O}_4/\text{N-HNMK-3}$ was designed and manufactured by means of a solvothermal method, using ordered N-doped mesoporous carbon (N-HNMK-3) as substrate, and then the bifunctional electrocatalytic performance corresponding to ORR, OER in alkaline media was carefully investigated. The results showed that $\text{Co}_3\text{O}_4/\text{N-HNMK-3}$ composite, a non-precious metal centered electrocatalyst, displayed excellent ORR performance (activity, selectivity, and stability) close to that of commercial 20 wt.% Pt/C and a promising OER activity near 20 wt.% RuO_2/C . The outstanding bifunctional activities of $\text{Co}_3\text{O}_4/\text{N-HNMK-3}$ was assessed with the lowest ΔE value of 0.86 V ($E_{\text{OER},10 \text{ mA cm}^{-2}} - E_{\text{ORR},-3 \text{ mA cm}^{-2}}$) with respect to the two commercial precious metal-based electrocatalysts.

Keywords: Ordered mesoporous carbon; nitrogen doping; cobalt-based electrocatalyst; bifunctional oxygen electrode; solvothermal method

1. Introduction

Hydrogen is deemed as the best way for renewable sources energy-storage to replace petroleum-based energy resources because of its high calorific value, abundant reserve, and near zero release. Yet, both the oxygen reduction reaction (ORR) and oxygen evolution reaction (OER) individually play crucial roles in fuel cells for the practical application of hydrogen, and water electrolysis for the high-efficiency production of high-purity hydrogen [1–4]. Recently, unitized regenerative cells (URCs), integrating water electrolysis and fuel cell in one setup, have attracted increasing attention due to potential applications in aviation, submarines and transportation as a mobile power source. This issue remains key to exploring high performance and low cost. In terms of electrocatalytic activity, Pt/C and Ru-/Ir oxides are generally considered to be the most advanced electrochemical oxygen catalysts for the ORR and OER processes, respectively. However, high cost, low methanol tolerance, and poor stability continue to hamper practical marketing development [5].

Therefore, it remains a big challenge to develop promising bifunctional oxygen electrodes for the development of URCs.

Among non-precious metal electrocatalysts being developed such as cobalt-based chalcogenides, CoSe_2 , CoS , and Co_3O_4 , show outstanding performance toward oxygen electrode reactions including activity, selectivity, and durability in alkaline media [6–9]. However, cobalt-based chalcogenide electrocatalysts have a low electrical conductivity and *per se* a negative effect on the performance of the electrocatalyst. On the other hand, ordered mesoporous carbon as a conductive substrate has attracted more attention because of large surface, high conductivity and long durability. [10–13]. In addition, the doping heteroatom, such as nitrogen [14,15], phosphor [16,17], sulfur [18] and boron [19], can further improve electrocatalytic performance towards oxygen electrode reactions due to new active species. In a previous report, we developed N-doped ordered mesoporous carbons (CMK-3) with high ORR activity, long stability, and outstanding methanol tolerance in 0.1 M KOH [20]. Therefore, it is possible to explore high-performance, low-cost electrocatalysts using N-doped ordered mesoporous carbon as a substrate to support cobalt-based chalcogenides.

Here, we manufactured the N-doped ordered mesoporous carbon substrate (N-HNMK-3) for Co_3O_4 composite ($\text{Co}_3\text{O}_4/\text{N-HNMK-3}$) by means of a solvothermal route using the home-made ordered mesoporous carbon as carbon source, melamine as a nitrogen source, cobalt acetate as a cobalt source, and urea as the precipitating agent. Figure 1 describes the corresponding synthesis process. In addition, we carefully examined the bifunctional electrocatalytic performance of ORR and OER processes in alkaline media using the rotating disc electrode technique. The compound, based on non-precious metals, shows a promising electrocatalytic performance.

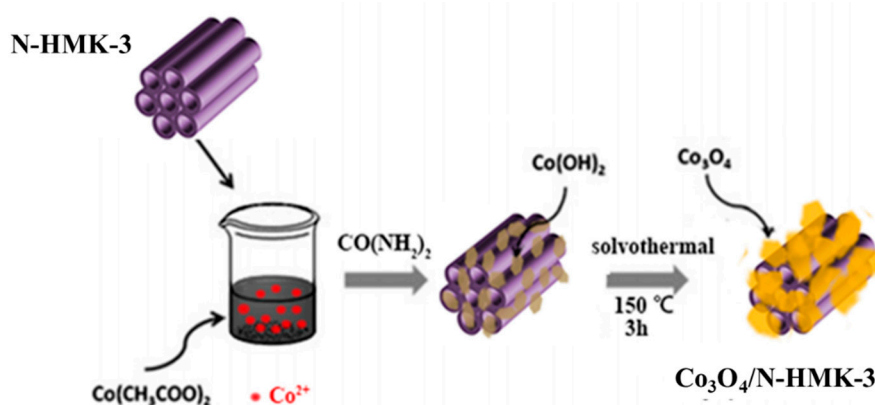


Figure 1. Schematic on preparation process of $\text{Co}_3\text{O}_4/\text{N-HNMK-3}$.

2. Materials and Methods

2.1. Chemicals

Cobalt acetate ($\text{Co}(\text{CH}_3\text{COO})_2 \cdot 6\text{H}_2\text{O}$), urea ($\text{CO}(\text{NH}_2)_2$), HNO_3 (6M), melamine ($\text{C}_3\text{H}_6\text{N}_6$), and ethanol ($\text{C}_2\text{H}_5\text{OH}$) were A.R. grade and were directly used as received from Beijing Chemical Co. Ltd (Beijing, China). CMK-3 was synthesized as reported previously [20].

2.2. Synthesis of Nitrogen-Doped Ordered Mesoporous Carbon (N-HNMK-3)

Nitrogen-doped ordered mesoporous carbon was fabricated by post-treated nitrogen doping method using ordered mesoporous carbon (CMK-3, surface area, $1247.5 \text{ m}^2/\text{g}$; pore volume, 1.5 mL/g) as carbon source, and melamine as nitrogen source. To obtain HNMK-3, CMK-3 (0.5002 g) was dispersed in 6.0 M HNO_3 (50.0 mL) under vigorous stirring at $70 \text{ }^\circ\text{C}$ for 3 h, and the resulting suspension was cleaned to neutral pH using deionized water. Thereafter, 0.5000 g HNMK-3 and 2.5000 g melamine were then mixed during grinding to form the homogeneous mixture. Finally, the

obtained mixture was calcined in a nitrogen atmosphere at 900 °C for 4 h to produce nitrogen-doped ordered mesoporous carbon (N-HNMK-3).

2.3. Synthesis of $\text{Co}_3\text{O}_4/\text{N-HNMK-3}$ Electrocatalyst

$\text{Co}_3\text{O}_4/\text{N-HNMK-3}$ electrocatalyst was carefully generated via the solvothermal route using N-HNMK-3 as conductive support; $\text{Co}(\text{CH}_3\text{COO})_2$ as cobalt source, and $\text{CO}(\text{NH}_2)_2$ as the precipitating agent. Typically, 0.0175 g of the as-prepared N-HNMK-3 was dispersed in ethanol (40.0 mL) by ultrasound for 2 h to form the suspension A. Simultaneously, 1.50 g $\text{Co}(\text{Ac})_2$ (6.0 mmol) was added in deionized water (40.0 mL) and ultra-sonicated for 20 min to form solution B. Then suspension A and solution B were mixed and ultrasonicated again to produce another suspension. At this point 0.72 g $\text{CO}(\text{NH}_2)_2$ was added under vigorous stirring at 80 °C for 24 h to produce a suspension, which was heated at 150 °C in a Teflon-lined stainless-steel autoclave for 3 h. The cooled product was centrifuged and washed with deionized water and ethanol three cycles, and dried at 60 °C overnight. The collected final product was $\text{Co}_3\text{O}_4/\text{N-HNMK-3}$. In addition, Co_3O_4 , as a reference, was prepared in the same procedure without N-HNMK-3.

2.4. Characterization

The materials phase was characterized by Rigaku Ultima III XRD (Rigaku Corporation, Tokyo, Japan) with $\text{Cu K}\alpha$ radiation ($\lambda = 0.154$ nm) at 5 min^{-1} per 2θ . The morphologies were analyzed by Zeiss Supra 55 SEM (Carl Zeiss Jena, Oberkochen, German), a JEOL JEM-2012 TEM (JEOL, Tokyo, Japan), and HRTEM (JEOL, Tokyo, Japan) with a line resolution of 0.19 nm was used. Raman spectra were examined via a Nanofinder 3.0 Raman spectrometer with a He-Ne laser beam of 532 nm. Binding energies of chemical species were collected by XPS using VG ESCALAB 2201 XL spectrometer (Thermo VG Scientific, West Sussex, England).

2.5. Electrochemical Measurements

All electrochemical tests were performed in a standard three-electrode system on the Chen Hua electrochemical workstation (CH Instruments Ins., Shanghai, China) at 25 °C. Here, a saturated calomel electrode and a Pt-wire were employed as the reference and counter electrodes, respectively. In this work, all potentials were referred to a reversible hydrogen electrode (RHE): $E_{\text{RHE}} = E_{\text{SCE}} + 0.99$ V (0.1 M KOH); and $E_{\text{RHE}} = E_{\text{SCE}} + 1.06$ V (1.0 M KOH).

Prior to catalyst deposition, the GC disk was polished with γ -alumina (5A), and successively ultra-sonically treated in water, and then ethanol for one min in each solvent. The ink was prepared by mixing the catalyst powder (6.7 mg), Nafion (5 wt.%) (40 μL), ethanol (300 μL), deionized water (1160 μL) and ultra-sonicated for 40 min. 4.2 μL of the ink was deposited onto the GC disk (4.0 mm, diameter) with a catalyst mass loading of $150 \mu\text{g cm}^{-2}$. The electrolyte was degassed with argon and oxygen for 30 min before cyclic voltammetry (CV) tests. Also, two benchmarks: 20 wt.% Pt/C (Johnson Matthey) and RuO_2/C were prepared as references with a corresponding loading of $60 \mu\text{g cm}^{-2}$ for Pt, and RuO_2 .

In the ORR test, the LSV curves were recorded in O_2 -saturated 0.1 M KOH by scanning the disc potential vs. RHE from 0.95 V to 0.15 V at 5 mVs^{-1} with the electrode rotated at 2500, 2025, 1600, 1225, 900, 625, and 400 rpm, and analysis performed using the Koutecky-Levich (K-L) equation:

$$\frac{1}{j} = \frac{1}{j_k} + \frac{1}{j_d} = \frac{1}{j_k} + \frac{1}{B\omega^{1/2}} \quad (1)$$

where:

$$B = 0.62nFC_0D_0^{2/3}\nu^{-1/6} \quad (2)$$

$$j_k = nFkC_0 \quad (3)$$

j , j_k , j_d are the corresponding measured, kinetic and diffusion limiting current densities, respectively [5]; C_0 and D_0 were the saturated concentration, and the diffusion coefficient of O_2 ($1.14 \times 10^{-6} \text{ mol cm}^{-3}$ and $1.73 \times 10^{-5} \text{ cm s}^{-1}$) in 0.1 M KOH, v was the kinetic viscosity coefficient ($0.01 \text{ cm}^2 \text{ s}^{-1}$).

In the RRDE test, the HO_2^- and the number of electrons transferred (n) was calculated by the following two equations:

$$HO_2^- \% = 200 * \frac{I_R/N}{I_D + I_R/N} \quad (4)$$

$$n = 4 * \frac{I_D}{I_D + I_R/N} \quad (5)$$

where I_D , I_R and N is disk current, ring current and collection efficiency (0.424), respectively.

For the OER tests, measurements were carried out in O_2 -saturated 1.0 M KOH with a rotating speed of 1600 rpm at a scan rate of 5 mV s^{-1} from 1.0 V to 1.65V *vs.* RHE.

3. Results and Discussion

3.1. Structure, Morphology, and Chemical Composition

Figure 2 shows the powder PXRD patterns of N-HNMK-3, Co_3O_4 , and Co_3O_4/N -HNMK-3. Compared to CMK-3, the peak of N-HNMK-3 samples at $23.8^\circ/2\theta$ shifts to a lower angle with a higher degree of graphitization, which could be the result of a change in electron distribution following the incorporation of the heteroatom on the surface of carbon materials [21]. Based on the Bragg equation, a series of Bragg reflection peaks in Co_3O_4 and Co_3O_4/N -HNMK-3 samples correspond to (111), (220), (311), (400), (511), and (440) crystal faces, that match well with the cubic spinel phase Co_3O_4 (ICDD PDF card No. 42-1467). This means that the urea-assisted solvothermal method is an available way to prepare the Co_3O_4/N -HNMK-3 composite.

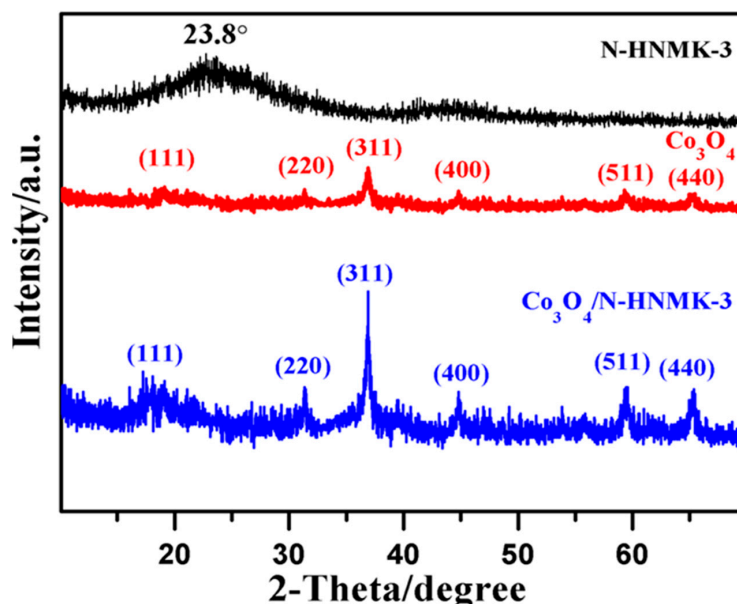


Figure 2. Powder XRD patterns of N-HNMK-3, Co_3O_4 , and Co_3O_4/N -HNMK-3 composite.

Figure 3 displays the morphologies and microstructures of Co_3O_4 and Co_3O_4/N -HNMK-3 samples. The Co_3O_4 sample shows different rod-shape in size, Figure 3a. In comparison, the Co_3O_4 particles, in Co_3O_4/N -HNMK-3 composite, are well-dispersed and supported on N-HNMK-3 substrate, Figure 3b,c. In addition, the average particle size for Co_3O_4 was 20–30 nm, Figure 3c. The HRTEM image of Co_3O_4 reveals three lattice distances such as 0.286, 0.244 and 0.202 nm, which individually correspond to (220), (311) and (400) Co_3O_4 crystal planes, Figure 3d.

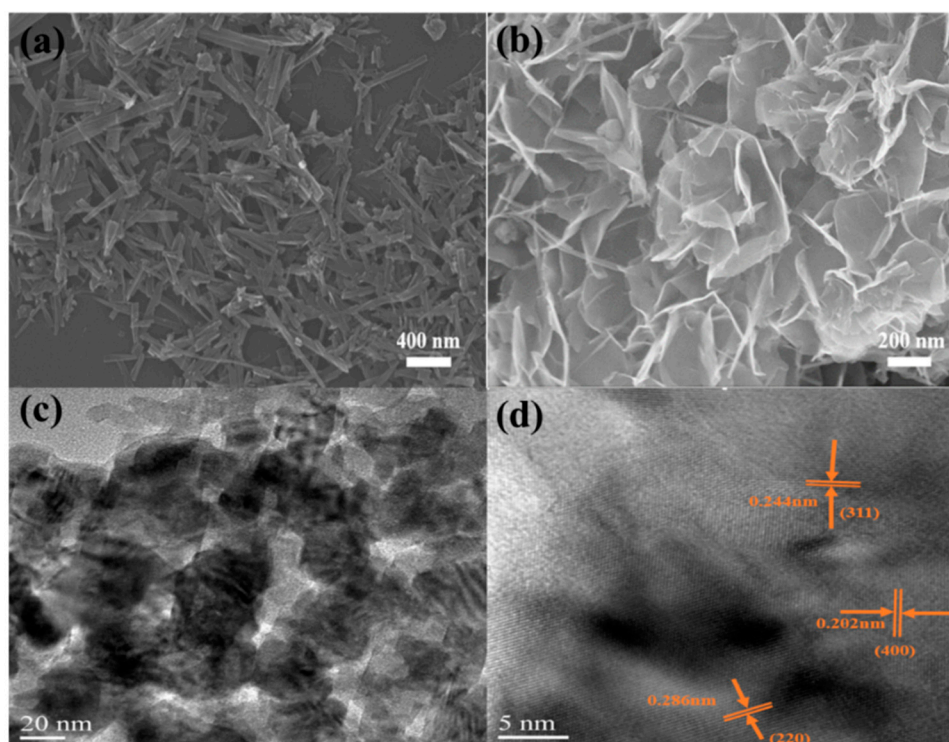


Figure 3. (a) The SEM images of Co_3O_4 , (b) $\text{Co}_3\text{O}_4/\text{N-HNMK-3}$. (c) TEM and (d) HRTEM images of $\text{Co}_3\text{O}_4/\text{N-HNMK-3}$.

In addition, Figure 4 shows the Raman spectra of N-HNMK-3, Co_3O_4 , and $\text{Co}_3\text{O}_4/\text{N-HNMK-3}$ samples as well as the corresponding fitting profiles of N-HNMK-3 and $\text{Co}_3\text{O}_4/\text{N-HNMK-3}$. One observes two characteristic bands for N-HNMK-3, and $\text{Co}_3\text{O}_4/\text{N-HNMK-3}$ centered at 1358 (D peak) and 1590 (G peak) cm^{-1} . The former peak (D peak) refers to sp^3 -like C atoms defect sites, whereas the latter (G peak) refers to sp^2 C=C stretching mode [22]. Remarkably, other peaks were detected at 192, 468, 516 and 677 cm^{-1} , assessing the presence of Co_3O_4 [23]. The intensity ratio of two bands ($I_{\text{D}}/I_{\text{G}}$) illustrates the disordered degree of carbonization. A ratio of 2.96 for N-HNMK-3, and 2.78 for $\text{Co}_3\text{O}_4/\text{N-HNMK-3}$ suggest that the incorporation of Co_3O_4 decreases the disordered degree, increasing the conductivity of the substrate.

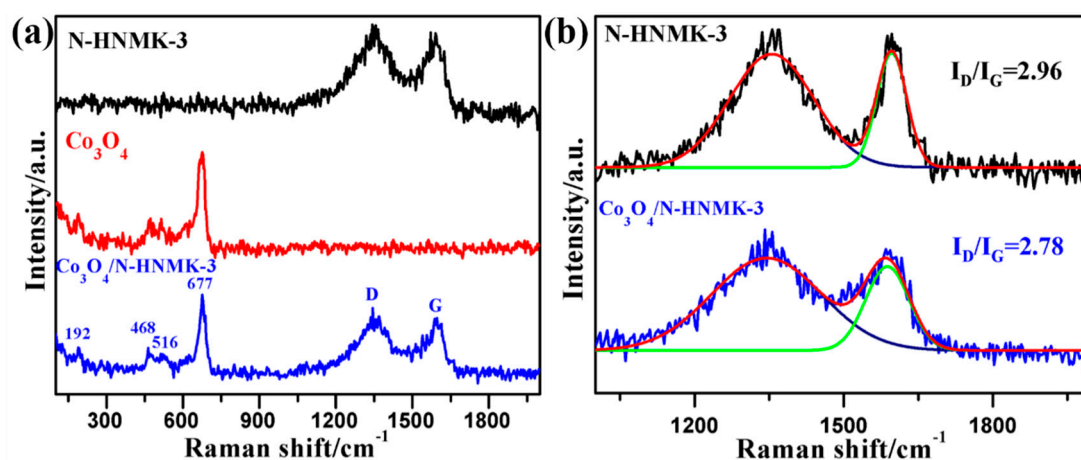


Figure 4. (a) Raman spectra of N-HNMK-3, Co_3O_4 and $\text{Co}_3\text{O}_4/\text{N-HNMK-3}$. (b) The corresponding Raman fitting profiles of N-HNMK-3 and $\text{Co}_3\text{O}_4/\text{N-HNMK-3}$.

Surface elemental properties and electronic valence states were further characterized by XPS. A survey spectrum of $\text{Co}_3\text{O}_4/\text{HNMK-3}$ displays the existence of C 1s, N 1s, O 1s, Co 2p signals at 284.5, 399.9, 530.5, 780.1 and 796.2 eV, respectively, as shown in Figure 5a. The corresponding atomic percentage of every element of different samples, N-HNMK-3 has a similar nitrogen content with $\text{Co}_3\text{O}_4/\text{HNMK-3}$, as summarized in Table 1. In the C1s high-resolution XPS spectrum, shown in Figure 5b, the prominent peak centered at 284.6 eV corresponds to sp^2 -hybridised carbon atoms in graphitic structure. The series of fitted peaks at 285.7, 288.3, and 288.6 eV are attributed to C=N, O=C=O and C-N, respectively. The XPS spectra of C=N and C-N further assess the presence of N-dopant atoms. As to Co2p spectrum, Figure 5c there are two peaks centered at 779.7 and 795.1 eV attributed to Co $2\text{p}_{3/2}$ and $2\text{p}_{1/2}$ signals, with an energy separation of 15.4 eV, evidencing the presence of Co_3O_4 in the composites [24]. Two nitrogen species detected in the N 1s high resolution, shown in Figure 5d, at ~ 398.6 eV and 400.2 eV are assigned to pyridine and Pyrrole-N. Previous results already demonstrated that pyridine N is an active site for the ORR [25]. The relative content of Pyrrole-N in $\text{Co}_3\text{O}_4/\text{HNMK-3}$ sample is 70.2%, which is higher than that of Pyridine-N (29.8%). It's worth noting that N-HNMK-3 and $\text{Co}_3\text{O}_4/\text{HNMK-3}$ samples have similar N content.

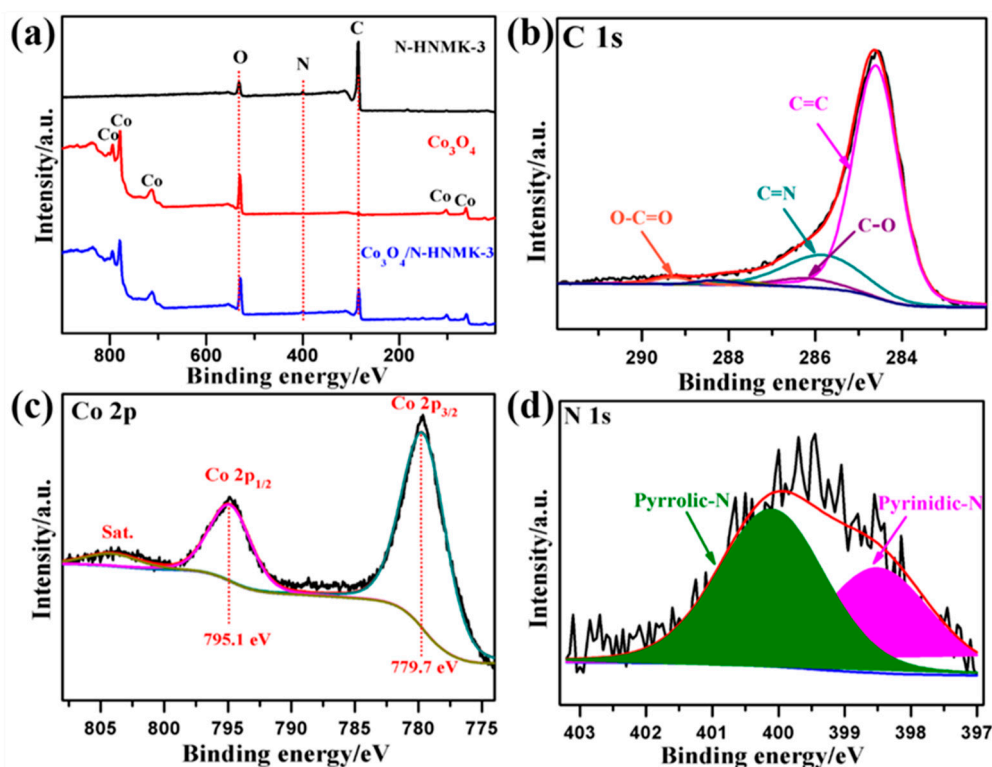


Figure 5. (a) XPS survey scan of samples: N-HNMK-3, Co_3O_4 and $\text{Co}_3\text{O}_4/\text{N-HNMK-3}$; XPS spectra of (b) C 1s; (c) Co 2p; (d) N 1s of $\text{Co}_3\text{O}_4/\text{N-HNMK-3}$.

Table 1. The element amount (at. %) in N-HNMK-3, Co_3O_4 and $\text{Co}_3\text{O}_4/\text{N-HNMK-3}$ samples.

Samples	C	N	Co	O	Pyridinic-N	Pyrrolic-N
N-HNMK-3	88.8	2.6		8.6	31.2	68.8
Co_3O_4			42.8	57.2		
$\text{Co}_3\text{O}_4/\text{N-HNMK-3}$	60.6	2.2	9.4	27.8	29.8	70.2

3.2. Electrocatalytic ORR Performance

The ORR performance of $\text{Co}_3\text{O}_4/\text{N-HNMK-3}$ composite was determined by RDE technique, and compared to two commercial reference materials: Pt/C and RuO_2/C . Figure 6 displays the activity

towards ORR in 0.1 M KOH electrolyte. Specifically, Figure 6a,b show the ORR activity difference among five samples: N-HNMK-3, physical mixture of N-HNMK-3 and Co_3O_4 , $\text{Co}_3\text{O}_4/\text{N-HNMK-3}$ composite, Pt/C, and RuO_2/C . Herein, it is observed that the $\text{Co}_3\text{O}_4/\text{N-HNMK-3}$ composite has a much higher ORR activity compared to N-HNMK-3, the physical mixture, and RuO_2/C , and close to Pt/C. Interestingly, the $\text{Co}_3\text{O}_4/\text{N-HNMK-3}$ composite shows much better ORR activity than the mechanical mixture ($\text{Co}_3\text{O}_4 + \text{N-HNMK-3}$). This difference in the ORR activity results from the possible synergistic effect between two compositions, and from the high dispersion of Co_3O_4 on the N-HNMK-3 substrate. In addition, cyclic voltammetry measurement, shown in Figure 6c, was conducted to gain deeper insight into the ORR process. In the O_2 -saturated electrolyte there is a cathodic peak centered at 0.75 V, which is absent in the Ar-saturated electrolyte. The onset potential of $\text{Co}_3\text{O}_4/\text{N-HNMK}$ was detected at 0.90 V *vs.* RHE. The ORR hydrodynamics on $\text{Co}_3\text{O}_4/\text{N-HNMK-3}$ between 400 rpm to 2500 rpm is shown in Figure 6d with well-defined sigmoidal curves. The electron transfers number (n) was estimated through the slopes of fitted K-L plots, see the inset in Figure 6d. Within the applied electrode potential from 0.2 to 0.5 V, the estimated transfer number (n) per O_2 molecule was ca. 3.94, suggesting a 4-electron transfer pathway. Meanwhile, we used the RRDE to calculate the hydrogen peroxide and electron transfer number in Figure S1 (See Supporting Information). The low hydrogen peroxide below 15% and transfer number beyond ca. 3.75 in the range of 0.1–0.75 V suggested a close 4-electron transfer pathway.

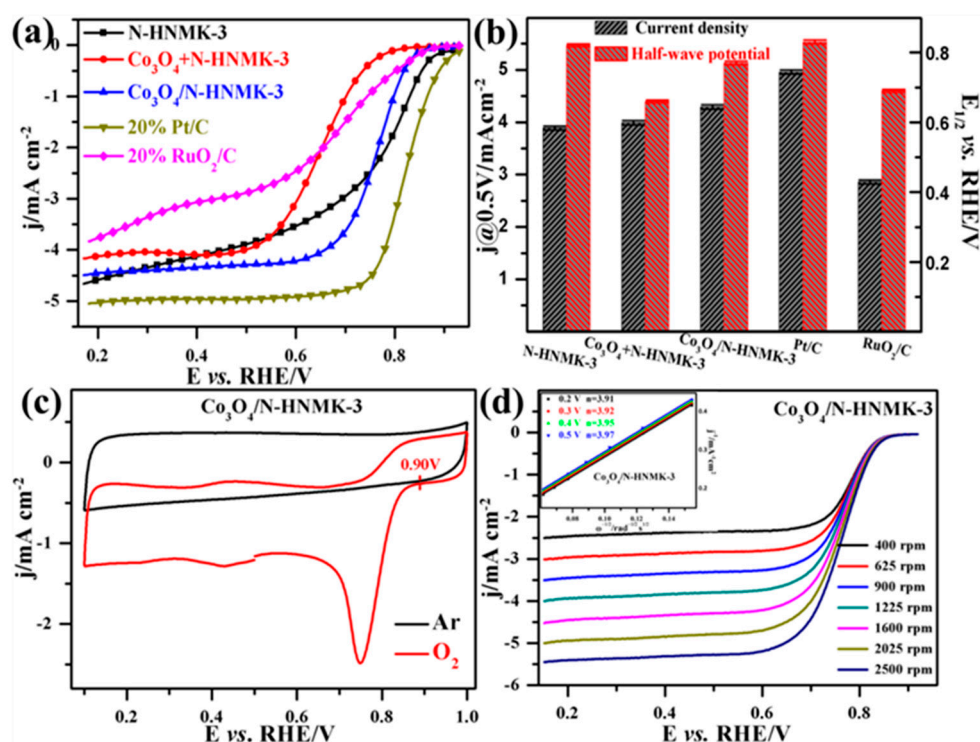


Figure 6. (a) ORR polarization curves of N-HNMK-3, $\text{Co}_3\text{O}_4 + \text{N-HNMK-3}$ (physical mixture), $\text{Co}_3\text{O}_4/\text{N-HNMK-3}$, Pt/C, and RuO_2/C at 1600 rpm in O_2 -saturated 0.1M KOH; (b) the limited current density at 0.50 V/RHE and half-wave potential from (a); (c) CV curves of $\text{Co}_3\text{O}_4/\text{N-HNMK-3}$ in Ar- and O_2 -saturated 0.1M KOH; (d) ORR polarization curves of $\text{Co}_3\text{O}_4/\text{N-HNMK-3}$ at various rotation rates, the inset shows the corresponding K-L plot of $\text{Co}_3\text{O}_4/\text{N-HNMK-3}$.

In addition to activity, the selectivity (tolerance to small organics) and the stability are two other key parameters for a high performance electrocatalyst. Figure 7a depicts the electrocatalytic selectivity in the presence and the absence of 3.0 M methanol in 0.1 M KOH electrolyte. After the addition of 3 M methanol, no significant change was observed in the polarization curves in Ar- and/or O_2 -saturated

electrolyte, see the inset in Figure 7a. In O₂-saturated electrolyte Co₃O₄/N-HNMK-3 showed a complete tolerance to methanol. In contrast, as it is well established, Pt/C has no selectivity towards the ORR in presence of methanol, since this material develops a mixed potential due to methanol oxidation and oxygen reduction. Furthermore, the stability test, as demonstrated by chronoamperometry, Figure 7b, was conducted at 0.70 V/RHE, and revealed that, after 18000 s, the ORR activity of Co₃O₄/N-HNMK-3 dropped 18.2% against 23.9% on Pt/C. Meanwhile, CVs with multiple cycles in oxygen-saturated solution for ORR were shown in Figure S2 (See Supporting Information), after the accelerated aging test, the reduction potential only shifts 36 mV to a negative region for 1500 cycles.

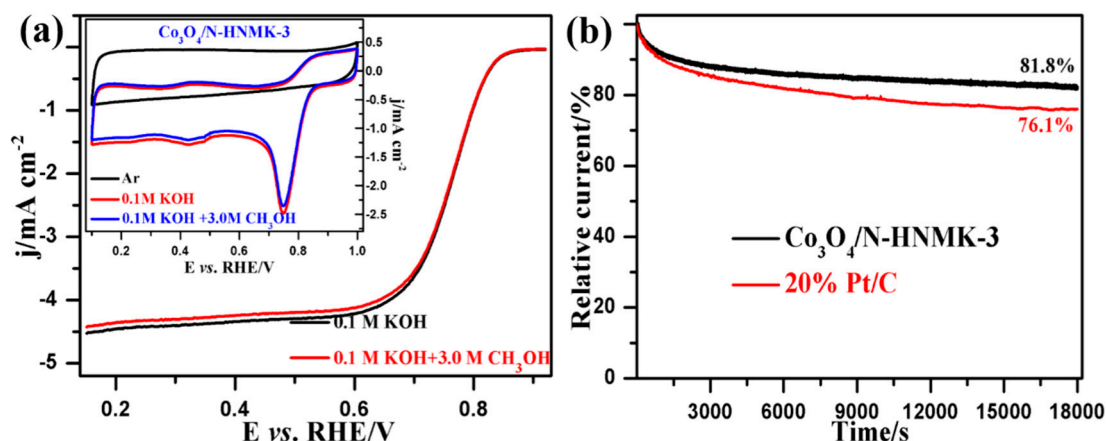


Figure 7. (a) CV and LSV curves of Co₃O₄/N-HNMK-3 in O₂-saturated with or without 3.0M methanol in 0.1 M KOH; (b) The durability test of Co₃O₄/N-HNMK-3 and 20 wt.% Pt/C at 0.70 V in O₂-saturated 0.1 M KOH at 1600 rpm.

3.3. Electrocatalytic OER Performance

The OER plays a crucial role in water electrolysis and metal-air batteries' systems [26]. In particular, high-performance OER electrocatalysts aim at reducing energy costs to produce high purity hydrogen and promote the development of URCs. Figure 8 shows the activity of Co₃O₄/N-HNMK-3 compared to N-HNMK-3, physical mixture of Co₃O₄ + N-HNMK-3, Pt/C, and RuO₂/C in 1.0 M KOH. Apart from RuO₂/C, the Co₃O₄/N-HNMK-3 has the highest OER activity with a higher current density of 19.56 mA cm⁻² at 1.65 V, lower overpotential (365 mV) at the current density of 10 mA cm⁻², a value close to the best OER electrocatalyst RuO₂/C. The Tafel plots for the OER kinetics are shown in Figure 8b. The slope of 93 mV dec⁻¹ for Co₃O₄/N-HNMK-3 is higher than that of 74 mV dec⁻¹ for RuO₂/C, and lower than that of the physical mixture. In addition, the OER stability test, via CV, performed on Co₃O₄/N-HNMK-3 is shown in Figure 8c,d. No significant variation was observed after 1500 cycles, and to some extent, Co₃O₄/N-HNMK-3 showed a ca. 4.1% increase in the overpotential at 10 mA cm⁻² after 1500 cycles. The results confirm that Co₃O₄/N-HNMK-3 is quite durable for the OER in 1.0 M KOH electrolyte.

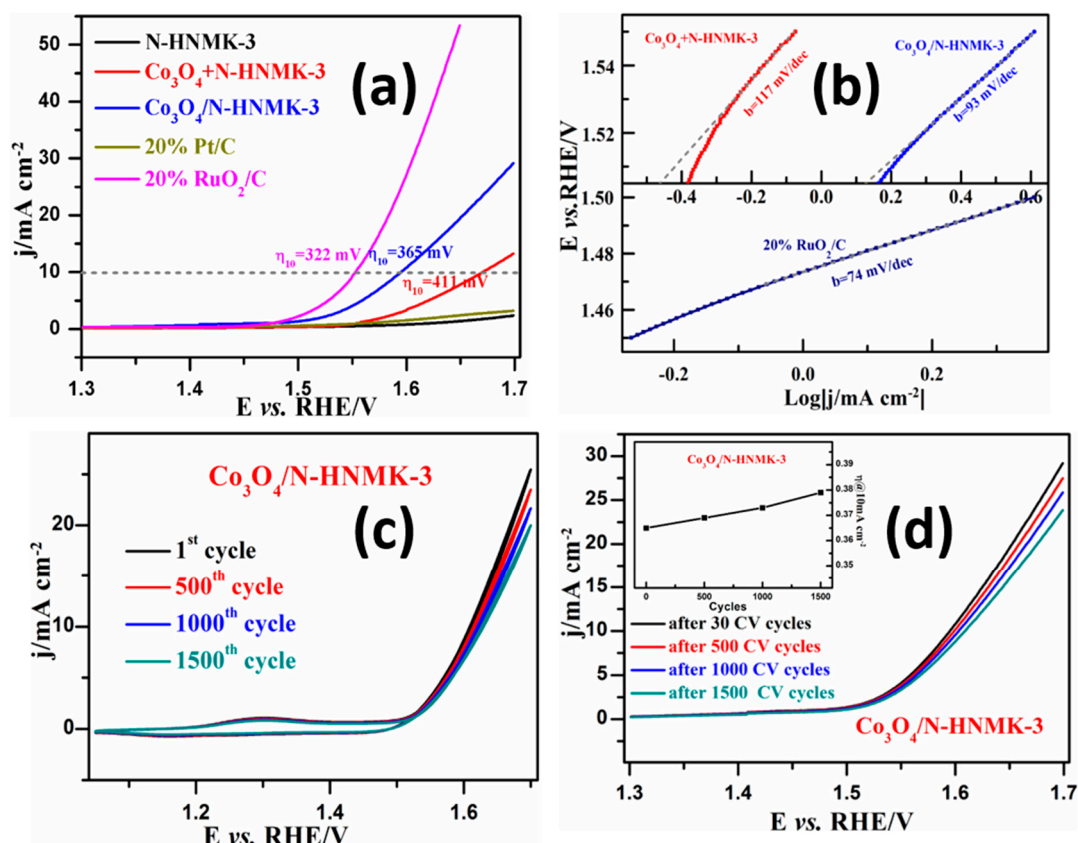


Figure 8. (a) LSV curves of N-HNMK-3, $\text{Co}_3\text{O}_4 + \text{N-HNMK-3}$ (physical mixture), $\text{Co}_3\text{O}_4/\text{N-HNMK-3}$, 20 wt.% Pt/C, and 20 wt.% RuO_2/C towards the OER in O_2 -saturated 1.0 M KOH at 5 mV s^{-1} and 1600 rpm; (b) Tafel plots of each samples derived from curves in (a); (c) CVs of $\text{Co}_3\text{O}_4/\text{N-HNMK-3}$ from 1.05 V to 1.70 V at 200 mV s^{-1} in O_2 -saturated 1.0 M KOH from 1st cycle to 1500th cycle; (d) LSV curves of $\text{Co}_3\text{O}_4/\text{N-HNMK-3}$ from 1.30 V to 1.70 V at 5 mV s^{-1} , the inset presents the variation of η_{10} at different CV cycles.

3.4. The Bifunctional ORR/OER Performance

The overvoltage between ORR and OER is an important parameter to evaluate the bifunctional electrocatalytic activity of the material. The corresponding data are summarized in Table 2. The ΔE value is defined as the difference in potential between the OER current density of 10.0 mA cm^{-2} and the ORR current density of -3.0 mA cm^{-2} . Among the listed catalysts [27–32] reported in the literature, $\text{Co}_3\text{O}_4/\text{N-HNMK-3}$ shows the best and promising bifunctional activity with a minimum ΔE value, which is attributed to the interaction developed between Co_3O_4 species onto N-doped ordered mesoporous carbons.

Table 2. The oxygen bifunctional electrocatalytic performance of catalysts prepared in this work compared with other bifunctional catalysts from the literature.

Catalysts	E vs. RHE at $j = -3 \text{ mA cm}^{-2}$	E vs. RHE at $j = 10 \text{ mA cm}^{-2}$	ΔE ($E_{\text{OER}@10 \text{ mA cm}^{-2}} - E_{\text{ORR}@-3 \text{ mA cm}^{-2}}$)	Refs.
N-HNMK-3	0.69	2.13	1.44	This work
Co ₃ O ₄ +N-HNMK-3	0.56	1.69	1.13	This work
Co ₃ O ₄ /N-HNMK-3	0.73	1.59	0.86	This work
20% Pt/C	0.81	2.07	1.26	This work
20% RuO ₂ /C	0.44	1.55	1.11	This work
Co ₃ O ₄ /Co ₂ MnO ₄	0.68	1.77	1.09	27
MnCo ₂ O ₄ /Nanocarbon	0.79	1.75	0.96	28
NiCo ₂ O ₄ /Graphene	0.60	1.68	1.08	29
CoFe ₂ O ₄ /Biocarbon	0.69	1.67	0.98	30
O-NiCoFe-LDH	0.62	1.67	1.05	31
Co(OH) ₂ CO ₃ /C	0.81	1.73	0.92	32

4. Conclusions

In this paper, a nitrogen-doped ordered mesoporous carbons supported Co₃O₄ composite (Co₃O₄/N-HNMK-3) was prepared through a solvothermal method. The Co₃O₄/N-HNMK-3 composite showed a much higher ORR performance, which was close to that of the commercial Pt/C in 0.1 M KOH. An excellent OER performance near commercial RuO₂/C in 1.0 M KOH was also obtained. Interestingly, Co₃O₄/N-HNMK-3 has outstanding bifunctional activity with a much lower ΔE value between $E_{\text{OER}@10 \text{ mA cm}^{-2}} - E_{\text{ORR}@-3 \text{ mA cm}^{-2}}$ as compared to Pt/C and RuO₂/C in alkaline medium. Undoubtedly, the synthesis method developed here to obtain the oxygen electrode based on Co₃O₄/N-HNMK-3, with non-precious metals will promote the practical development of fuel cells, water electrolysis and unitized regenerative cells.

Supplementary Materials: The following are available online at <http://www.mdpi.com/2571-9637/2/2/18/s1>, Figure S1. (a) Ring (top) and disk (down) current density from RRDE measurements of Co₃O₄/N-HNMK-3 samples after annealing at different temperature in O₂-saturated 0.1 M KOH at 25 °C with a sweep rate of 5 mV s⁻¹ at a rotating speed of 1600 rpm; (b) Molar fraction of HO₂⁻ formation and electron transfer number n from rotating ring-disk electrode (RRDE) curves in (a). Figure S2. (a) CVs of Co₃O₄/N-HNMK-3 from 0.1 V to 1.0 V at 100 mV s⁻¹ in O₂-saturated 0.1 M KOH from 1st cycle to 1500th cycle; (b) LSVs of Co₃O₄/N-HNMK-3 from 0.1 V to 1.0 V at 5 mV s⁻¹ in O₂-saturated 0.1 M KOH from 1st cycle to 1500th cycle.

Author Contributions: Methodology, N.A.-V. and Y.F.; formal analysis, S.Z., G.Y. and H.Z.; investigation, J.W.; writing—original draft preparation, J.W. and S.Z.; writing—review and editing, N.A.-V., D.L., P.T., and Y.F.; supervision, Y.F.; project administration, Y.F.

Acknowledgments: This work is supported by the National Natural Science Foundation of China, and the Fundamental Research Funds for the Central Universities (12060093063). H.H. Zhong specially thanks the financial support from China Scholarship Council (201806880040).

Conflicts of Interest: The authors declare no conflict of interest.

References

1. Carmo, M.; Fritz, D.L.; Mergel, J.; Stolten, D. A comprehensive review on PEM water electrolysis. *Int. J. Hydrogen* **2013**, *38*, 4901–4934. [CrossRef]
2. Postole, G.; Auroux, A. The poisoning level of Pt/C catalysts used in PEM fuel cells by the hydrogen feed gas impurities: The bonding strength. *Int. J. Hydrogen* **2011**, *36*, 6817–6825. [CrossRef]
3. Zhang, X.; Chan, S.H.; Ho, H.K.; Tan, S.-C.; Li, M.; Li, G.; Li, J.; Feng, Z. Towards a smart energy network: The roles of fuel/electrolysis cells and technological perspectives. *Int. J. Hydrogen* **2015**, *40*, 6866–6919. [CrossRef]
4. Qiao, S.Z.; Jiao, Y.; Zheng, Y.; Jaroniec, M. Design of electrocatalysts for oxygen- and hydrogen-involving energy conversion reactions. *Chem. Soc. Rev.* **2015**, *44*, 2060–2086.
5. Sui, S.; Wang, X.; Zhou, X.; Su, Y.; Riffat, S.; Liu, C.-J. A comprehensive review of Pt electrocatalysts for the oxygen reduction reaction: Nanostructure, activity, mechanism and carbon support in PEM fuel cells. *J. Mater. Chem. A* **2017**, *5*, 1808–1825. [CrossRef]

6. Feng, Y.; He, T.; Alonso-Vante, N. In situ free-surfactant synthesis and ORR-electrochemistry of carbon-supported Co_3S_4 and CoSe_2 nanoparticles. *Chem. Mater.* **2007**, *20*, 26–28. [[CrossRef](#)]
7. Xu, X.; Liang, H.; Ming, F.; Qi, Z.; Xie, Y.; Wang, Z. Prussian Blue Analogues Derived Penroseite $(\text{Ni},\text{Co})\text{Se}_2$ Nanocages Anchored on 3D Graphene Aerogel for Efficient Water Splitting. *ACS Catal.* **2017**, *7*, 6394–6399. [[CrossRef](#)]
8. Zhong, H.; Campos-Roldán, C.A.; Zhao, Y.; Zhang, S.; Feng, Y.; Alonso-Vante, N. Recent Advances of Cobalt-Based Electrocatalysts for Oxygen Electrode Reactions and Hydrogen Evolution Reaction. *Catalysts* **2018**, *8*, 559. [[CrossRef](#)]
9. Jia, X.; Gao, S.; Liu, T.; Li, D.; Tang, P.; Feng, Y. Controllable Synthesis and Bi-functional Electrocatalytic Performance towards Oxygen Electrode Reactions of $\text{Co}_3\text{O}_4/\text{N-RGO}$ Composites. *Electrochim. Acta* **2017**, *226*, 104–112. [[CrossRef](#)]
10. Tan, H.; Li, Y.; Jiang, X.; Tang, J.; Wang, Z.; Qian, H.; Mei, P.; Malgras, V.; Bando, Y.; Yamauchi, Y. Perfectly ordered mesoporous iron-nitrogen doped carbon as highly efficient catalyst for oxygen reduction reaction in both alkaline and acidic electrolytes. *Nano Energy* **2017**, *36*, 286–294. [[CrossRef](#)]
11. Shen, H.; Gracia-Espino, E.; Ma, J.; Tang, H.; Mamat, X.; Wagberg, T.; Hu, G.; Guo, S. Atomically FeN_2 moieties dispersed on mesoporous carbon: A new atomic catalyst for efficient oxygen reduction catalysis. *Nano Energy* **2017**, *35*, 9–16. [[CrossRef](#)]
12. Jiang, T.; Wang, Y.; Wang, K.; Liang, Y.; Wu, D.; Tsiakaras, P.; Song, S. A novel sulfur-nitrogen dual doped ordered mesoporous carbon electrocatalyst for efficient oxygen reduction reaction. *Appl. Catal. B: Environ.* **2016**, *189*, 1–11. [[CrossRef](#)]
13. Ferrero, G.A.; Fuertes, A.B.; Sevilla, M.; Titirici, M.-M.; Solis, M.S. Efficient metal-free N-doped mesoporous carbon catalysts for ORR by a template-free approach. *Carbon* **2016**, *106*, 179–187. [[CrossRef](#)]
14. Zhang, J.; Zhao, Z.; Xia, Z.; Dai, L. A metal-free bifunctional electrocatalyst for oxygen reduction and oxygen evolution reactions. *Nat. Nanotechnol.* **2015**, *10*, 444–452. [[CrossRef](#)]
15. Mengxia, S.; Changping, R.; Yan, C. Covalent entrapment of cobalt-iron sulfides in N-doped mesoporous carbon: Extraordinary bifunctional electrocatalysts for oxygen reduction and evolution reactions. *ACS Appl. Mater. Interfaces* **2015**, *7*, 1207.
16. Lei, W.; Deng, Y.-P.; Li, G.; Cano, Z.P.; Wang, X.; Luo, D.; Liu, Y.; Wang, D.; Chen, Z. Two-Dimensional Phosphorus-Doped Carbon Nanosheets with Tunable Porosity for Oxygen Reactions in Zinc-Air Batteries. *ACS Catal.* **2018**, *8*, 2464–2472. [[CrossRef](#)]
17. Chai, G.-L.; Qiu, K.; Qiao, M.; Titirici, M.-M.; Shang, C.; Guo, Z.X. Active sites engineering leads to exceptional ORR and OER bifunctionality in P,N Co-doped graphene frameworks. *Environ. Sci.* **2017**, *10*, 1186–1195. [[CrossRef](#)]
18. Patra, S.; Choudhary, R.; Roy, E.; Madhuri, R.; Sharma, P.K.; Sharma, D.P.K. Heteroatom-doped graphene 'Idli': A green and foody approach towards development of metal free bifunctional catalyst for rechargeable zinc-air battery. *Nano Energy* **2016**, *30*, 118–129. [[CrossRef](#)]
19. Han, J.-S.; Chung, D.Y.; Ha, D.-G.; Kim, J.-H.; Choi, K.; Sung, Y.-E.; Kang, S.-H. Nitrogen and boron co-doped hollow carbon catalyst for the oxygen reduction reaction. *Carbon* **2016**, *105*, 1–7. [[CrossRef](#)]
20. Zhong, H.; Zhang, S.; Jiang, J.; Feng, Y. Improved Electrocatalytic Performance of Tailored Metal-Free Nitrogen-Doped Ordered Mesoporous Carbons for the Oxygen Reduction Reaction. *ChemElectroChem* **2018**, *5*, 1899–1904. [[CrossRef](#)]
21. Zhao, X.; Wang, A.; Yan, J.; Sun, G.; Sun, L.; Zhang, T. Synthesis and Electrochemical Performance of Heteroatom-Incorporated Ordered Mesoporous Carbons. *Chem. Mater.* **2010**, *22*, 5463–5473. [[CrossRef](#)]
22. Granozzi, G.; Balbuena, P.B.; Ma, J.; Habrioux, A.; Luo, Y.; Ramos-Sanchez, G.; Calvillo, L.; Alonso-Vante, N. Electronic interaction between platinum nanoparticles and nitrogen-doped reduced graphene oxide: Effect on the oxygen reduction reaction. *J. Mater. Chem. A* **2015**, *3*, 11891–11904.
23. Wang, C.; Shi, P.; Yao, W. Synergistic effect of Co_3O_4 nanoparticles and graphene as catalysts for peroxydisulfate-based orange II degradation with high oxidant utilization efficiency. *J. Phys. Chem. C* **2016**, *120*, 336–344. [[CrossRef](#)]
24. Wu, Z.-S.; Ren, W.; Wen, L.; Gao, L.; Zhao, J.; Chen, Z.; Zhou, G.; Li, F.; Cheng, H.-M. Graphene Anchored with Co_3O_4 Nanoparticles as Anode of Lithium Ion Batteries with Enhanced Reversible Capacity and Cyclic Performance. *ACS Nano* **2010**, *4*, 3187–3194. [[CrossRef](#)]

25. Liu, Y.; Ai, K.; Lu, L. Polydopamine and Its Derivative Materials: Synthesis and Promising Applications in Energy, Environmental, and Biomedical Fields. *Chem. Rev.* **2014**, *114*, 5057–5115. [[CrossRef](#)]
26. Gorlin, Y.; Jaramillo, T.F. A Bifunctional Nonprecious Metal Catalyst for Oxygen Reduction and Water Oxidation. *J. Am. Chem. Soc.* **2010**, *132*, 13612–13614. [[CrossRef](#)] [[PubMed](#)]
27. Wang, D.; Chen, X.; Evans, D.G.; Yang, W. Well-dispersed $\text{Co}_3\text{O}_4/\text{Co}_2\text{MnO}_4$ nanocomposites as a synergistic bifunctional catalyst for oxygen reduction and oxygen evolution reactions. *Nanoscale* **2013**, *5*, 5312. [[CrossRef](#)]
28. Ge, X.; Liu, Y.; Goh, F.W.T.; Hor, T.S.A.; Zong, Y.; Xiao, P.; Zhang, Z.; Lim, S.H.; Li, B.; Wang, X.; et al. Dual-Phase Spinel MnCo_2O_4 and Spinel MnCo_2O_4 /Nanocarbon Hybrids for Electrocatalytic Oxygen Reduction and Evolution. *ACS Appl. Mater. Interfaces* **2014**, *6*, 12684–12691. [[CrossRef](#)] [[PubMed](#)]
29. Lee, D.U.; Kim, B.J.; Chen, Z. One-pot synthesis of a mesoporous NiCo_2O_4 nanoplatelet and graphene hybrid and its oxygen reduction and evolution activities as an efficient bi-functional electrocatalyst. *J. Mater. Chem. A* **2013**, *1*, 4754. [[CrossRef](#)]
30. Liu, S.; Bian, W.; Yang, Z.; Tian, J.; Jin, C.; Shen, M.; Zhou, Z.; Yang, R. A facile synthesis of CoFe_2O_4 /biocarbon nanocomposites as efficient bi-functional electrocatalysts for the oxygen reduction and oxygen evolution reaction. *J. Mater. Chem. A* **2014**, *2*, 18012–18017. [[CrossRef](#)]
31. Qian, L.; Lu, Z.; Xu, T.; Wu, X.; Tian, Y.; Li, Y.; Huo, Z.; Sun, X.; Duan, X. Ternary Layered Double Hydroxides as High-Performance Bifunctional Materials for Oxygen Electrocatalysis. *Adv. Mater.* **2015**, *5*, 1500245. [[CrossRef](#)]
32. Wang, Y.; Ding, W.; Chen, S.; Nie, Y.; Xiong, K.; Wei, Z. Cobalt carbonate hydroxide/C: An efficient dual electrocatalyst for oxygen reduction/evolution reactions. *Chem. Commun.* **2014**, *50*, 15529–15532. [[CrossRef](#)] [[PubMed](#)]



© 2019 by the authors. Licensee MDPI, Basel, Switzerland. This article is an open access article distributed under the terms and conditions of the Creative Commons Attribution (CC BY) license (<http://creativecommons.org/licenses/by/4.0/>).